Inside the hysteresis loop: Multiplicity of internal states in confined fluids

Alexander V. Neimark,* Peter I. Ravikovitch, and Aleksey Vishnyakov

TRI/Princeton, 601 Prospect Avenue, Princeton, New Jersey 08542
(Received 31 October 2001; published 1 March 2002)

We study the equilibrium and stability of metastable states and capillary condensation hysteresis of a Lennard-Jones fluid in cylindrical pores by means of the canonical ensemble density functional theory and gauge cell Monte Carlo simulations. We demonstrate a possibility for the existence of multiple laterally uniform internal states of equal density inside the hysteresis loop. The region of multiple states is bounded by the states of zero compressibility. The internal states can be stabilized in Monte Carlo simulations constraining the density fluctuations.

The rapid development of nanotechnologies, especially synthesis and modification of novel nanostructured materials [1,2] has catalyzed increasing attention of theoreticians and experimentalists to the problems of phase equilibria and transitions in confined fluids [3–13]. Vapor sorption and capillary condensation in nanopores are prominent examples of phenomena in confined fluids, which offer a variety of intriguing features, such as, the multiplicity of equilibrium stable and metastable states and hysteresis [3–16]. It is well documented that sorption and desorption isotherms typically do not coincide, yet they form a reproducible hysteresis loop [16]. In geometrically disordered confinements, as shown both experimentally [16] and theoretically [13], sequential changes of the stages of sorption and desorption lead to the scanning of multiple equilibrium states inside the hysteresis loop. However, thermodynamic analysis of these states is hindered due to the system complexity. In this paper, we show that even in a single pore of a symmetric shape there is a possibility for the existence of multiple states of equal density inside the hysteresis loop. These states were found first by means of the mean field density functional theory (DFT), and then confirmed by the Monte Carlo (MC) simulation with the example of capillary condensation of Lennard-Jones (LJ) fluids in cylindrical nanopores [17].

DFT is a proven tool for analyses of sorption and phase transitions in pores [18–20]. In the pioneering papers [14,15], one can find a qualitative description of the capillary condensation phenomenon as a first-order phase transition characterized by the shift of the conditions of criticality, phase coexistence and spinodals compared to the bulk fluid. It was shown that the nonlocal DFT [18–20] agrees with MC simulations [3,4,21–23], and also with reference experiments [3,4,24–28]. To analyze the behavior of a system in the hysteresis region, we employ the canonical ensemble version of the density functional theory (CEDFT) [29]. In contrast to the conventional DFT, which implies the grand canonical ensemble minimization at given volume, temperature, and chemical potential [18–20], we find equilibrium states of a fluid within a pore of a given shape provided that the mean fluid density $\langle \rho \rangle$ is fixed, the pore volume V is unchanged and the system is embedded in a bath of constant temperature T. Thus, we deal with a closed system of a fixed volume

at isothermal conditions, whose equilibrium states are defined by minimization of the Helmholtz free energy, represented as a functional $F[\rho(\mathbf{r})]$ of the spatially varying fluid density $\rho(\mathbf{r})$, in the canonical ensemble at constant $\langle \rho \rangle, V$, and T [30]. To find a solution to this conditional extremum problem, one has to introduce a Lagrange multiplier μ, as an additional unknown parameter and solve the Euler equation given by $\mu = \delta F[\rho(\mathbf{r})]/\delta\rho(\mathbf{r})$. Here, $\delta/\delta\rho$ denotes the functional derivative. The solution gives the equilibrium density profile $\rho(\mathbf{r},\langle \rho \rangle,T)$ and the value of $\mu(\langle \rho \rangle,T)$, which turns out to be equal to the chemical potential of the corresponding state. In the following calculations we consider a LJ fluid in a cylindrical pore using the smoothed density approximation [18–20] to represent the Helmholtz free energy functional, $F[\rho(\mathbf{r})]$. Solutions to the Euler equation were obtained by using the Broyden [31] method. To demonstrate the multiplicity of internal states on the simplest system, we intentionally constrict ourselves to studies of laterally uniform configuration and perform minimization over the laterally uniform density profiles $\rho(\mathbf{r}) = \rho(r)$, where r is the distance from the pore center. It is known that in sufficiently long cylindrical pores may exist various nonuniform configurations comprised of sequences of liquid lenses/bridges and bubbles as shown in MC and MD silulations of binary liquids [32–34]. A detailed description of the density functional and parameters employed can be found elsewhere [23].

In Fig. 1 we present a series of the CEDFT isotherms in cylindrical pores of different diameters. The fluid-fluid and fluid-solid parameters were chosen to reproduce Ar sorption at 87 K ($kT/\epsilon = 0.74$) in the channels of siliceous mesoporous molecular sieves of the MCM-41 type. This choice was motivated by the availability of relevant experimental data [24–28]. This example is typical for a first-order vapor-liquid phase transition. In the narrowest pore of 1.31 nm in width, we observe a supercritical behavior: the isotherm is monotonous and consists of stable equilibrium states. As the pore size increases above the critical size, the isotherms take upon a sigmoid, van der Waals'-type shape with multiple equilibrium states. We distinguish three regions on the subcritical isotherm, as shown in Fig. 2 with the example of the isotherm in 3.15 nm pore. The adsorption branch OS_V corresponds to the consecutive formation of adsorption layers associated with sigmoid swings indicating layering transitions. Since the fluid density in the pore center is of the order of the vapor density, the states on the adsorption branch are
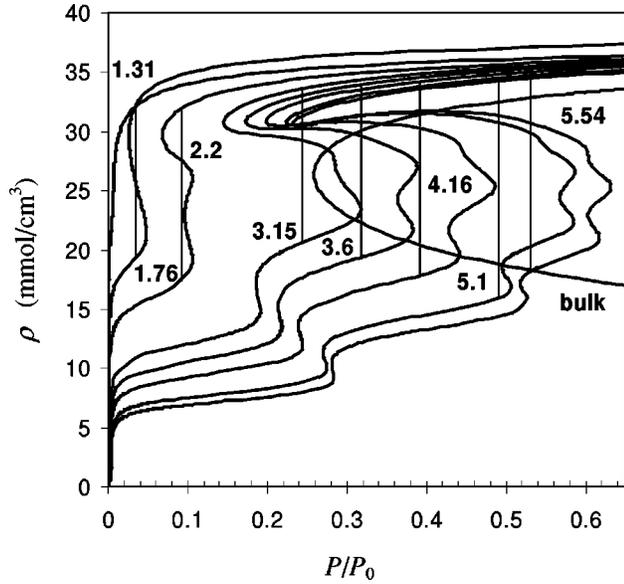
*Email address: aneimark@triprinceton.org

FIG. 1. Adsorption isotherms of Ar in cylindrical pores at 87.3 K ($kT/\epsilon = 0.74$) plotted as the fluid density ρ versus the bulk pressure reduced to the saturation pressure P/P_0. Internal pore diameters increase from left to right and are shown in the plot (in nm). The portion of the bulk liquid isotherm in the undersaturation conditions is presented for comparison. The leftmost isotherm in a 1.31-nm pore is supercritical. The isotherms in wider pores have the characteristic sigmoid shape with the multiple states. Vertical lines indicate the positions of the equilibrium vapor-liquid transitions.

referred to as vaporlike states. The desorption branch $S_L H$ corresponds to liquidlike states of condensed fluid. The descending trajectory $S_L S_V$ corresponds to the states that we call internal states. The internal states can be stabilized in the
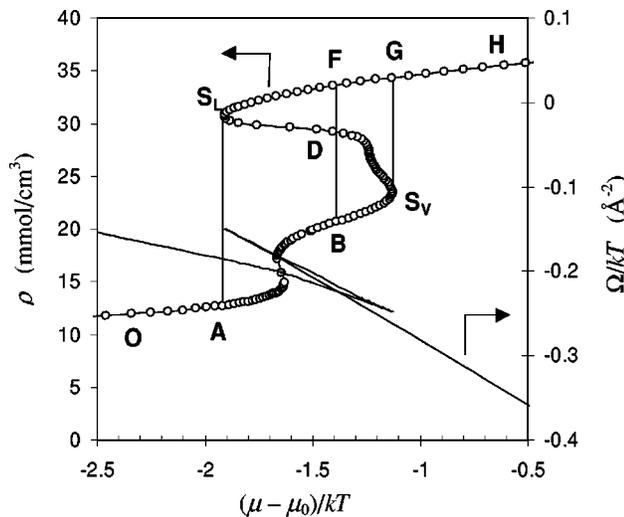

FIG. 2. Adsorption isotherm of Ar in a 3.15-nm cylindrical pore ($R = 5.17\sigma$) at 87.3 K ($kT/\epsilon = 0.74$) plotted as the density ρ versus the reduced chemical potential μ. The zigzag line shows the changes in the grand thermodynamic potential of the system. The intersection point corresponds to the phase coexistence (points B and F on the isotherm); the turnover points correspond to the vaporlike (S_V) and liquidlike (S_L) spinodals.

closed system of a finite volume but they are unstable in the open system, and, therefore, cannot be observed in a real experiment, in which unrestricted mass exchange with the environment is allowed. Albeit the compressibility of the internal states is negative, they can be generated in molecular simulations by suppressing density fluctuations in the system [11,35,36]. The possibility of obtaining such states in experiments with a limited bulk reservoir was discussed in Ref. [37].

The position of phase coexistence, points B and F of equilibrium transitions, complies with Maxwell's rule of equal areas, $\int_{\rho_B(\mu_e)}^{\rho_F(\mu_e)} \mu d\rho = \mu_e(\rho_F - \rho_B)$. Here, μ_e is the chemical potential of the equilibrium capillary condensation transition. Thus, at $\mu < \mu_e$, the vaporlike states are stable and the liquidlike states are metastable, and vise versa, at $\mu > \mu_e$, the liquidlike states are stable and the vaporlike states are metastable. The turnover points, S_V and S_L, correspond to the true limits of stability of vaporlike and liquidlike metastable states, respectively. In analogy with the bulk vapor-liquid phase diagram, we refer to these points as the vaporlike and liquidlike spinodals. The vaporlike spinodal S_V is the point of spontaneous capillary condensation. At this point, the adsorption layer becomes unstable, the energy barrier separating the metastable and stable states vanishes, and the system must jump onto the desorption branch under any experimental conditions at which the pore space is connected with a reservoir of vapor. Similarly, the liquidlike spinodal S_V is the point of spontaneous evaporation: The metastable condensed fluid becomes unstable and cavitates at any experimental conditions, and the system must jump onto the adsorption branch.

In pores wider than ~ 4 nm, we observe a phenomenon that, likely, has not been reported earlier. On the backward trajectory of the isotherm appears a region of multiple internal states of equal mean density, as shown in Fig. 3 with the example of the isotherm in 5.1 nm pore. The region of multiple states of equal mean density is bounded by the states of zero compressibility, S_{SL} and S_{SU}. These, physically unrealizable states first discussed in Ref. [11], were named superspinodals. The lower (S_{SL}) and upper (S_{SU}) superspinodals bound the range of fluid densities in which at a given temperature the Euler equation has three solutions with the same density and different chemical potentials: One state is located on the descending region $S_{SU} K$ of the backward trajectory adjoining to the vaporlike spinodal S_V; the second state may be either a liquidlike state on the branch $S_L R$, or an internal state on the descending region $S_L S_{SL}$ of the backward trajectory adjoining to the liquidlike spinodal S_L; the third, intermediate state lies on the ascending region $S_{SL} S_{SU}$ of the backward trajectory between the superspinodals. Note that a solution of the variation problem does not necessarily correspond to a minimum of the Helmholtz free energy potential $F[\rho(\mathbf{r})]$ with respect to the local variations of fluid density and, consequently, to an equilibrium state of the closed system. The condition of minimum, $[\delta^2 F[\rho(\mathbf{r})]/\delta\rho(\mathbf{r})^2]_{\langle\rho\rangle} > 0$, is apparently fulfilled in the case of the unique solution. However, in the case of multiple solutions, the condition of minimum has to be tested to distinguish the unstable states.
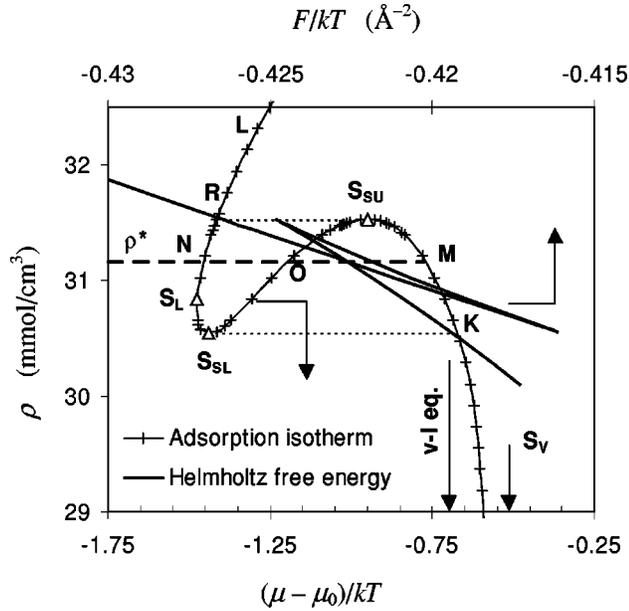
FIG. 3. Enlargement of the region of multiple internal states on the adsorption isotherm of Ar in a 5.1-nm cylindrical pore ($R = 8.125\sigma$) at 87.3 K ($kT/\epsilon = 0.74$). The isotherm is plotted as the fluid density ρ versus the reduced chemical potential $\mu - \mu_0$. The zigzag line shows the changes in the Helmholtz free energy F, (solid line) along the isotherm. The states M and N of equal Helmholtz free energy and equal density ρ^* are obtained by the Maxwell construction of equal areas. The states with $\rho < \rho^*$ between the vaporlike spinodal $S_V (\mu - \mu_0 = -0.522$, $N = 26.6$ mmol/cm^3, outside of the figure field) and point M, and states with $\rho > \rho^*$ between points N and L are intrinsically stable and correspond to the minimums of the Helmholtz free energy. The states between point M and the upper superspinodal S_{SU}, and the states between the lower superspinodal S_{SL} and point N are intrinsically metastable. The virtual states between the superspinodals S_{SL} and S_{SU} are entirely unstable and correspond to the maximums in the Helmholtz free energy. R is the liquidlike state of the same density as the upper superspinodal state S_{SU}; K is the internal state of the same density as the lower superspinodal state S_{SL}. Vertical arrow shows position of the equilibrium vapor-liquid transition at $\mu - \mu_0 = -0.696$.

In Fig. 3 we present the variation of the Helmholtz free energy along the isotherm calculated by integrating along the continuous trajectory in the region of multiple states. We see that the states on the ascending region between the superspinodals have a higher Helmholtz free energy than the two other states of the same mean density and, therefore, must correspond to the maximums of $F[\rho(\mathbf{r})]$. These states are entirely unstable: Local variations of the fluid density would drive the system to one of the states of the same density, which correspond to the minimums of $F[\rho(\mathbf{r})]$ and represent either stable or metastable states in the closed system. The Maxwell-type construction of equal areas in Fig. 3, $\oint_{\rho^*} \mu d\rho$, determines the density ρ^* separating the stable and metastable internal states. That is, the internal states on the branch $S_V M$ and the liquidlike states of $\rho > \rho_{SL}$ are stable, whereas the states on the regions $M S_{SU}$ and $S_{SL} N$ are metastable. To avoid a misinterpretation, we stress that here we deal with the stability of a closed system with respect to the internal
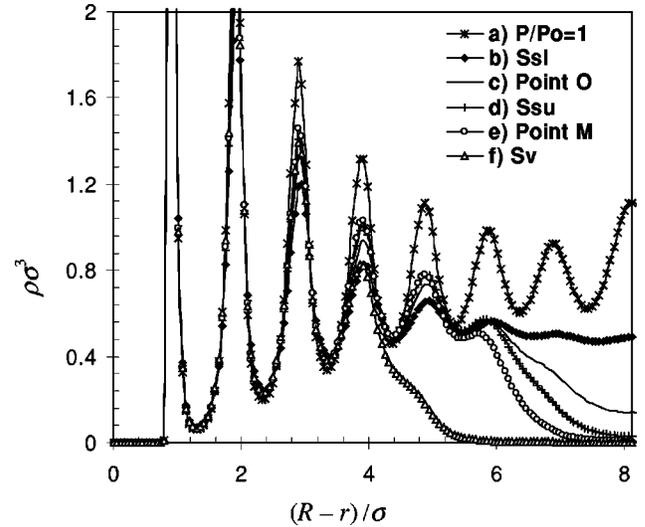

FIG. 4. Density profiles of Ar in a 5.1-nm cylindrical pore ($R = 8.125\sigma$) at 87.3 K ($kT/\epsilon = 0.74$) corresponding to (see Fig. 3)(a) Stable liquidlike state at the bulk saturation pressure $P/P_0 = 1$; (b) lower superspinodal point S_{SL}; (c) virtual state O; (d) upper superspinodal point S_{SU}; (e) intrinsically stable internal state at point M; (f) vaporlike spinodal S_V. Note that internal states are characterized by a thick liquidlike film with a well-defined interface or, in other words, by a bubble in the pore center.

degrees of freedom. In an open system, the internal states are unstable (for descending regions of the isotherm, $\partial^2 F/\partial \langle \rho \rangle^2 < 0$) unless specially stabilized by certain constrains. These internal states can be referred to as intrinsically stable states. It is worth noting that this analysis is reminiscent of the discussion in Ref. [38] regarding the stability of liquid droplets forming unduloids and lenses in cylindrical pores. The authors distinguished two types of stability: the Laplace stability with respect to the deformation of the droplet shape at a constant volume/mass and the Kelvin stability with respect to the mass exchange with the vapor phase. Using the above introduced terminology, the Laplace stability corresponds to the intrinsic stability of internal states in a closed isothermal system.

The states between the superspinodals are virtual states that cannot be stabilized by any external forces and would not be achievable in experiments and molecular simulations. This justifies the term superspinodal for the virtual state of zero compressibility ($|\partial^2 F/\partial \langle \rho \rangle^2| \to \infty$), which was introduced in Ref. [11] is a paraphrase of the definition of the spinodal for the state of diverging compressibility ($\partial^2 F/\partial \langle \rho \rangle^2 = 0$). Indeed, while the spinodal represents the true limit of the stability of the metastable states in the open system, the superspinodal represents the true limit of stabilization of the internal states that can be sampled by means the gauge cell MC simulation method [11], see below.

In Fig. 4 we demonstrate the molecular structure of the internal states. Between the vaporlike spinodal S_V and the upper superspinodal S_{SU}, the internal states correspond to the layer-by-layer growth of the adsorbed film. The density in the near-wall adsorbed layers reduces in accord with the decrease in the equilibrium pressure, as clearly seen for the
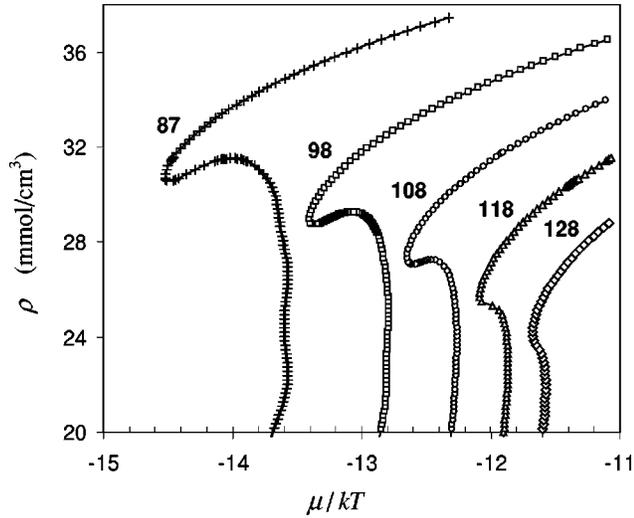
FIG. 5. Adsorption isotherms of Ar in a 5.1-nm cylindrical pore at different temperatures. The isotherms are plotted as the fluid density $\langle\rho\rangle$ versus the absolute chemical potential μ. Temperatures increase from left to right and are shown in the plot (in K). The superspinodal critical temperature T_{SS} is estimated between 108 and 118 K.
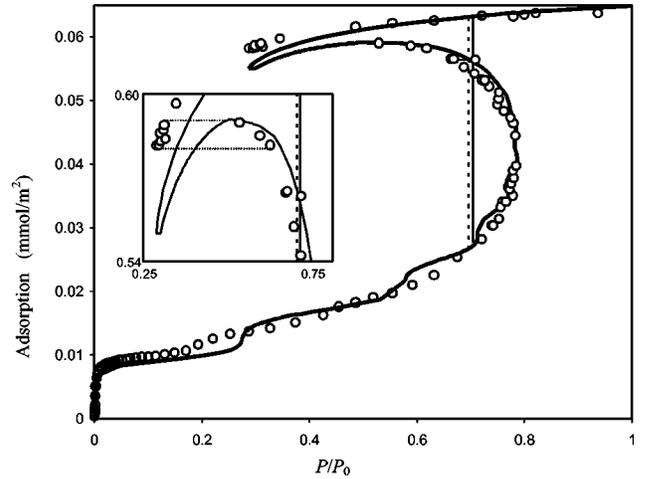

FIG. 6. Adsorption isotherms of nitrogen in cylindrical pores at 77.4 K ($kT/\epsilon=0.762$) plotted as the fluid density $\langle\rho\rangle$ versus the bulk pressure reduced to the saturation pressure P/P_0. The points represent the MC data and the continuous curve represents the DFT isotherm. Vertical lines correspond to the equilibrium vapor-liquid transition obtained by DFT (solid line) and MC (dashed line). Enlargement of the vicinity of the liquidlike spinodal demonstrates the existence of states of equal density. The gap in the MC trajectory indicates the region of unstable states between the superspinodals.

third layer. As the density increases, a thin vaporlike axisymmetric bubble in the central part of the pore shrinks (lines e and d on Fig. 4). The trajectory of the virtual states represents the gradual filling of the pore center without layering (lines d, c, and b on Fig. 4). The shape of the isotherm in the vicinity of the liquidlike spinodal changes qualitatively as the pore size increases. Instead of a rounded shape (Fig. 2), which can be approximated by a parabola, the isotherm tends to form a pronounced tongue (Fig. 1). The lower superspinodal S_{SL} approaches the liquidlike S_L spinodal. For a given pore, the shape of the isotherm also depends on temperature. As the temperature increases, the hysteresis loop becomes narrower and disappears at a certain pore critical temperature T_{pc}, which is smaller than the bulk critical temperature T_c. The phenomenon of the shift of criticality in confined fluids is well known [1,39–42]. In Fig. 5, we show the temperature dependence of the backward trajectory of internal states in 5.1 nm pore. As the temperature increases, the region of virtual states becomes narrower and at a certain superspinodal critical temperature, $T_{ss}<T_{pc}$, the lower and upper superspinodals coincide. At T_{ss}, the backward trajectory has one inflection point characterized by zero compressibility. At higher temperatures, the backward trajectory monotonously decreases and consists of intrinsically stable internal states.

To validate the results of the mean field theory, we have purposely searched for the multiple internal states by means of the gauge cell MC simulations [11]. In the gauge cell MC method [11], the simulation is performed simultaneously in two cells, which are in chemical equilibrium at isothermal conditions. Mass exchange between the cells is allowed; however, the cell volumes are kept unchanged. One of the cells represents the pore and the other is the gauge cell of a limited capacity. The fluid in the gauge cell is stable at the conditions of simulations ($\partial^2 F_g/\partial\langle\rho_g\rangle^2>0$, the subscript "$g$" denotes the gauge cell fluid) and serves as a reference.

The limited capacity of the gauge cell constrains the density fluctuations in the pore and allows one to keep the fluid in the pore in a state, which would be unstable in contact with the bulk. Indeed, the condition of stability of the total system is given by $(V_g/V)\partial^2 F/\partial\langle\rho\rangle^2+\partial^2 F_g/\partial\langle\rho_g\rangle^2>0$. Thus, choosing the ratio of the gauge cell and pore volumes, V_g/V, sufficiently small, we can stabilize and sample the states of negative compressibility. Approaching the superspinodals ($\partial^2 F/\partial\langle\rho\rangle^2\rightarrow\infty$) the stabilization condition fails. For the details of the gauge cell method, see Ref. [11].

MC simulations in cylindrical pores were performed in relatively short cells with periodic boundary conditions to prevent the formation of nonuniform configurations. Multiple laterally uniform internal states have been found, yet in larger pores than those presented in Fig. 1. In Fig. 6, we present an example of MC simulations of sorption equilibrium of a LJ fluid in a 9-nm-wide cylindrical pore. The fluid-fluid and fluid-solid parameters were chosen to reproduce nitrogen sorption at 77 K ($kT/\epsilon=0.762$) on silica [23]. The switchover from argon to nitrogen was motivated by the availability of relevant experimental data, which was shown to agree quantitatively with DFT and MC simulations of adsorption hysteresis [4]. In the vicinity of the liquidlike spinodal, the backward trajectory of internal states is nonmonotonic and discontinuous. The gap is interpreted as the region between the superspinodals: the density of pore fluid to the right exceeds the density to the left. The density of the pore fluid in the vicinity of the superspinodal point is determined with the accuracy of 0.05% and the bulk pressure with the accuracy of $\sim$5% by averaging over 5×10^7 configurations.

The DFT isotherm is in remarkable agreement with the MC data, including the positions of the vaporlike and liquidlike spinodals and phase equilibrium. As the parameters of
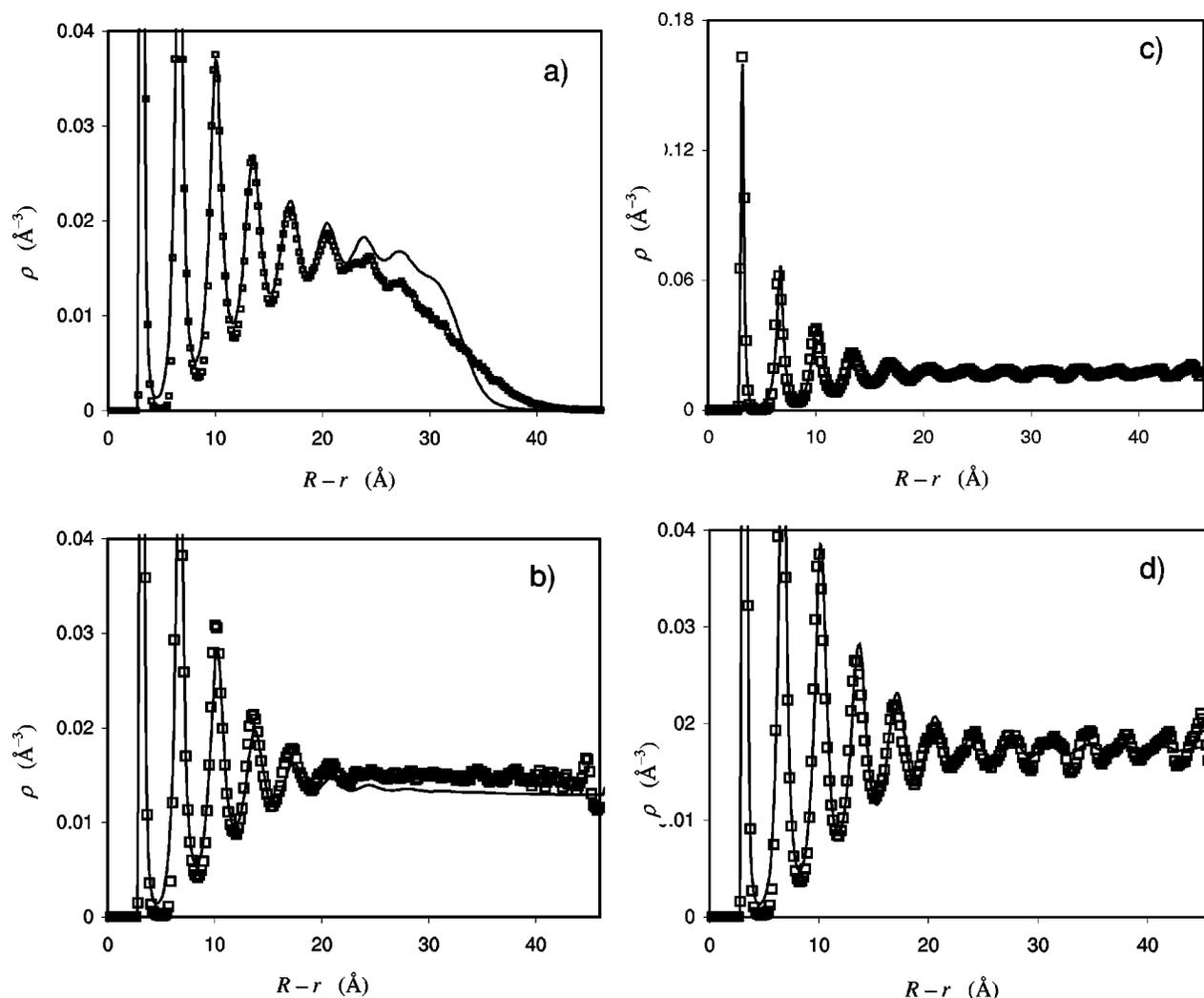
FIG. 7. Nitrogen density profiles in 9.0-nm pore at 77.4 K. Lines, CEDFT; squares, MC simulations (see Fig. 4 for description). (a) Upper superspinodal S_{SU}, (b) liquidlike spinodal, (c) liquidlike state at vapor-liquid equilibrium, (d) liquid state at $P = P_0$. Note a different scale in (d).

both models were chosen to represent the liquid density of bulk nitrogen [23], the densities of the liquidlike states on the desorption branch are almost equal, although DFT predicts a larger compressibility than that observed in MC simulations. Even the backward, descending trajectories between the vaporlike spinodal and the lower superspinodal practically coincide. Due to the discontinuity of the MC isotherm, the condition of phase equilibrium in the MC simulation was determined by the thermodynamic integration method by constructing a supercritical isotherm [43]. As it was expected, the DFT exaggerate the layering transitions along the adsorption branch and the superspinodal behavior producing the states of larger compressibility in the vicinity of liquidlike spinodal. These deviations are caused by the neglect of local lateral fluctuations in the DFT model employed [23].

The MC local density profiles of nitrogen in a 9- nm pore, given in Fig. 7, are qualitatively similar to those presented in Fig. 4. In overall, agreement between the DFT and MC density distributions is excellent. DFT predicts a sharper interface between the adsorbed film and vaporlike bubble than
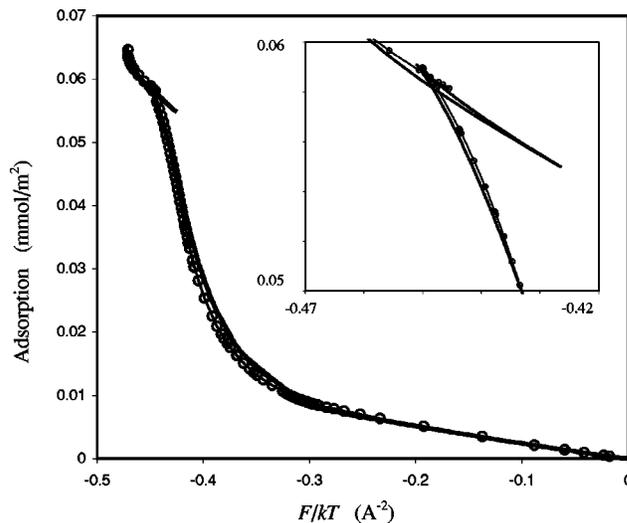

FIG. 8. Helmholtz free energies of nitrogen in a 9.0-nm pore at 77.4 K. The inset enlarges the superspinodal region.

MC. Also, notable difference is observed between the MC and DFT density profiles at the liquidlike spinodal, since DFT shows a lower fluid density at the spinodal point. In Fig. 8, we show the variation of the Helmholtz free energy F and estimate the density that determines the limits of intrinsically stable internal states. The Helmholtz free energies obtained by the MC and DFT methods agree well including the region of multiple internal states [Fig. 8(b)], although MC predicts higher fluid densities in that region.

Thus, the MC simulation confirms that the existence of multiple internal states of equal density is not an artifact of the mean field theory. This behavior may be observed in nanopores and other finite volume systems. Unachievable in a quasiequilibrium experiment with continuously varying external thermodynamic parameters, the internal states can be constructed by equilibrating under suitable constrains and consecutive quenching a specially prepared initial nonequilibrium state of a given density or composition, particularly in regular nanopores of mesoporous molecular sieves [1,2].

[1] *Nanoporous Materials II*, edited by A. Sayari, M. Jaroniec, and T. J. Pinnavaia, Studies in Surface Science and Catalysis Vol. 129 (Elsevier, Amsterdam, 2000).

[2] P. J. F. Harris, *Carbon Nanotubes and Related Structures: New Materials for the Twenty-First Century* (Cambridge University Press, Cambridge, 1999).

[3] P.I. Ravikovitch, S.C. O'Domhnaill, A.V. Neimark, F. Schüth, and K.K. Unger, Langmuir **11**, 4765 (1995).

[4] A.V. Neimark, P.I. Ravikovitch, and A. Vishnyakov, Phys. Rev. E **62**, R1493 (2000).

[5] K. Morishige and M. Shikimi, J. Chem. Phys. **108**, 7821 (1998).

[6] R. Radhakrishnan and K.E. Gubbins, Phys. Rev. Lett. **79**, 2847 (1997).

[7] L.D. Gelb, K.E. Gubbins, R. Radhakrishnan, and M. Sliwinska-Bartkowiak, Rep. Prog. Phys. **62**, 1573 (1999).

[8] M.W. Cole *et al.*, Phys. Rev. Lett. **84**, 3883 (2000).

[9] F. Restagno, L. Bocquet, and T. Biben, Phys. Rev. Lett. **84**, 2433 (2000).

[10] L. Sarkisov and P.A. Monson, Langmuir **16**, 9857 (2000).

[11] A.V. Neimark and A. Vishnyakov, Phys. Rev. E **62**, 4611 (2000).

[12] A. Vishnyakov and A.V. Neimark, J. Phys. Chem. B **105**, 7009 (2001).

[13] E. Kierlik, P.A. Monson, M.L. Rosinberg, L. Sarkisov, and G. Tarjus, Phys. Rev. Lett. **87**, 055701 (2001).

[14] R. Evans, U. Marini Bettolo Marconi, and P. Tarazona, J. Chem. Phys. **84**, 2376 (1986).

[15] R. Evans, U. Marini Bettolo Marconi, and P. Tarazona, J. Chem. Soc., Faraday Trans. 2 **82**, 1763 (1986).

[16] D. H. Everett, in *The Solid-Gas Interface*, edited by E. A. Flood (Marcel Dekker, New York, 1967), Vol. 2.

[17] Cylindrical pores studied here are examples of finite volume systems in which the thermodynamic limit and, correspondingly, the true phase equilibrium are not achievable. They have finite length and cannot be considered as one dimensional.

[18] P. Tarazona, Phys. Rev. A **31**, 2672 (1985).

[19] P. Tarazona, U. Marini Bettolo Marconi, and Mol. Phys. **60**, 573 (1987).

[20] R. Evans, in *Fundamentals of Inhomogeneous Fluids*, edited by D. Henderson (Marcel Dekker, New York, 1992), Chap. 5.

[21] B. K. Peterson *et al.*, J. Chem. Phys. **88**, 6487 (1988).

[22] C. Lastoskie, K.E. Gubbins, and N. Quirke, Langmuir **9**, 2693 (1993).

[23] P.I. Ravikovitch, A. Vishnyakov, and A.V. Neimark, Phys. Rev. E **64**, 011602 (2000).

[24] P.I. Ravikovitch, D. Wei, W.T. Chuen, G.L. Haller, A.V. Neimark, J. Phys. Chem. B **101**, 3671 (1997).

[25] A.V. Neimark, P.I. Ravikovitch, M. Grün, F. Schütz, and K. Unger, J. Colloid Interface Sci. **207**, 159 (1998)

[26] P.I. Ravikovitch, G.L. Haller, and A.V. Neimark, Adv. Colloid Interface Sci. **77**, 203 (1998).

[27] P.I. Ravikovitch and A.V. Neimark, Stud. Surf. Sci. Catal. **129**, 597 (2000)

[28] P.I. Ravikovitch and A.V. Neimark, Microporous Mater. **44-45**, 697 (2001).

[29] A.V. Neimark and P.I. Ravikovitch, in *Microscopic Simulation of Interfacial Phenomena in Solids and Liquids*, edited by S. R. Phillpot *et al.*, Mater. Res. Soc. Symp. Proc. **492** (Materials Research Society, Pittsburg, 1998), p. 27.

[30] We do not consider here situations of extreme confinement with a small number of molecules, for which the results of the grand canonical and canonical ensembles may differ. See, e.g., J.A. White, A. Gonzalez, F.L. Roman, and S. Velasco, Phys. Rev. Lett. **84**, 1220 (2000).

[31] W. H. Press, S. A. Teulkovsky, W. T. Vetterling, and B. P. Flannery, *Numerical Recipies in C* (Cambridge University Press, Cambridge, 1992).

[32] A.J. Liu, D.J. Durian, E. Herbolzheimer, and S.A. Safran, Phys. Rev. Lett. **65**, 1897 (1990).

[33] Z. Zhang and A. Chakrabarti, Phys. Rev. E **50**, R4290 (1994).

[34] L.D. Gelb and K.E. Gubbins, Physica A **244**, 112 (1997).

[35] A. De Keizer, T. Michalski, and G.H. Findenegg, Pure Appl. Chem. **63**, 1495 (1991).

[36] V.Y. Gusev, in *Microscopic Simulation of Interfacial Phenomena in Solids and Liquids* (Ref. [29]), p. 35.

[37] D. Everett, Colloids Surf., A **141**, 279 (1998).

[38] D.H. Everett and J.M. Haynes, J. Colloid Interface Sci. **38**, 125 (1972).

[39] R. Evans, U.M.B. Marconi, and P. Tarazona, J. Chem. Phys. **84**, 2376 (1986).

[40] C.G.V. Burgess, D.H. Everett, and S. Nuttall, Pure Appl. Chem. **61**, 1845 (1989).

[41] K. Morishige and M. Shikimi, J. Chem. Phys. **108**, 7821 (1998).

[42] A. Vishnyakov *et al.*, Langmuir **17**, 4451 (2001).

[43] B.K. Peterson and K.E. Gubbins, Mol. Phys. **6**, 215 (1987).